ELSEVIER

Chemical Engineering Journal 77 (2000) 57–63

Chemical Engineering Journal

www.elsevier.com/locate/cej

Measurement of bulk particulates on belt conveyor using dielectric tomography ☆

R.A. Williams *, S.P. Luke, K.L. Ostrowski, M.A. Bennett[1]

Camborne School of Mines, University of Exeter, Redruth, Cornwall TR15 3SE, UK

Abstract

We investigate the feasibility of using an array of non-invasive tomographic sensors around a moving conveyor belt carrying solid particulates. Results from experimental and simulated data show the importance of the position of electrode placement and the effect of the properties of the conveyor belt material itself. Use of the measurements to provide a continuous measurement of powder profile, surface fractal dimension, voidage, through time integration, and mass hold up is discussed. ©2000 Elsevier Science S.A. All rights reserved.

Keywords: Belt conveying; Capacitance tomography; Dielectric constant; Fractal dimension; Mass flow

1. Introduction

Conveying of fine powders, granulated and coarse rock is of significant importance in a range of industrial and manufacturing operations. In quarrying and mining of industrial minerals production the particulates may vary in size from 0.5 m to 100 μm. Plastics, polymers and waste reprocessing materials range from 50 mm to 500 μm. For fine chemical and pharmaceuticals, sizes from 10 mm to 10 μm may be transported. The research reported in this paper seeks to demonstrate the feasibility of using a non-invasive capacitance tomography sensor system to perform measurements on belts. This method can provide an image of the dielectric constant directly in a cross section. The objective is to evaluate if such a system could provide information on powder mass flow rate and additional information from which parameters describing the physical characteristics of the particulates themselves can be inferred. Measured features might be:

- instantaneous voidage of the particulate bed;
- instantaneous shape profile of the particulate heap, including surface fractal dimension;
- integrated mass flow rate (derived from the above and knowledge of belt speed); and
- parameters that describe variations in the voidage and surface profile with time, and hence the consistency of the upstream operation.

Some of the applications for this knowledge are obvious, but we seek also to assess the viability of using new information as a means of gaining a quantitative understanding of the process stage upstream of the conveyor (e.g. a crusher) and the consequences downstream for the next stage of the process (e.g. separator, screen) or the final customer.

2. Experimental arrangement

2.1. Electrical measurement method

Electrical capacitance tomography (ECT) is becoming widely used as a rapid and robust tool to provide data for an analysis of various multiphase systems [1]. To date the typical applications have included, for example, measurements of solids conveying, powder fluidisation, trickle-bed reactors and oil/water/gas transport [1–7]. The measurement method has been described in detail elsewhere [1] and consists of placing a number (typically 8–16) of electrode plates around the process (e.g. pipe) to be examined. These electrodes may be placed on the outer wall if the pipe is fabricated from electrically insulating material or can be embedded within the wall. By exciting the electrodes, for example by rapidly charging one electrode and measuring charge on another electrode, and repeating the procedure for every electrode-pair combination, these measurements can be reconstructed to form an image of the distribution of dielectric properties — this can be exploited in solids handling since the dielectric constant of the materials is larger than

☆ The authors are members of The Virtual Centre for Industrial Process Tomography.

* Corresponding author. Tel.: +44-1209-714866.

E-mail addresses: williams@csm.ex.ac.uk (R.A. Williams), r.a.williams@leeds.ac.uk (R.A. Williams).

[1] Current address: School of Process, Environmental and Material Engineering, University of Leeds, Leeds, LS2 9JT, UK. Tel.: +44-1132-332789.

1385-8947/00/$ – see front matter
PII: S1385-8947(99)00146-1

Table 1
Typical values of dielectric constant (ε) for some dry materials used in the work reported here (25°C, frequency = 10^6 Hz)

Calcium carbonate	6.1
Ceramics (clays)	5–7
Quartz	4.3
Silicone resin	3.8
Plexiglass	2.8–3.4

air ($\varepsilon = 1$). For cases of mineral particulates, the dielectric content typically lies in the range of 4–7 and for plastics 2–3.7. The reconstruction process is subject to a number of simplifying assumptions since no direct analytical solution to the three dimensional electric field equations is tractable [8]. To date methods have sought to linearise the complex non-linear response using back projection algorithms in combination with calibration of the measurement system often under static conditions. Other reconstruction methods may be used, for instance, employing iterative reconstruction schemes and model-based reconstruction protocols.

A commercially available ECT system was used (Process Tomography, Wilmslow) which consists of an electronics unit that provides fast (ca. 7000 measurement per second) and accurate (with an error of order 0.1 fF) measurements of the capacitance for the independent electrodes connections. The 'quality' of reconstructed image, irrespective of the applied reconstruction method, is determined by the amount of information on the electrostatic field in the sensing area, hence the number of electrodes is of importance. Since velocity of the moving belt in a belt conveyor is typically performed at a moderate speed, the process could be regarded as *static* during the measurement time that is required to collect data to assemble for one image (frame). The analysis presented here is based on the performance of the 12 electrode sensor (66 measurements per one frame) which provides a resolution of ≈5%. This value means that the size of the target object should be at least 5% of the sensor diameter assuming there is a large enough difference of dielectric constant between the object and the surrounding medium. Typically, the rate of data capture for an on-line ECT system may exceed 100 frames per second (Table 1).

2.2. Sensor installation around the belt

Fig. 1 shows a schematic diagram of the laboratory experimental arrangement in which electrodes are placed around a circular plastic former (pipe section). The conveyor belt passes through the sensor ring. The laboratory systems considered static tests (described below) using a small scale system comprising a rubber belt 0–0.5 m long and having a maximum width of 60 mm. Granular silica (mean size 200 μm) was placed on the bed, compacted by tapping, and then the profile of the solids was adjusted by sculpting or by running a profiled former along the length of the belt. Different profiles of the solids bed/air interface could thus be generated consistently along the length of the belt. The profiles corresponded to a set of curved profiles given by changes coefficients in a Fourier series, in which the solid/gas interface is expressed by a function $f(x)$, where

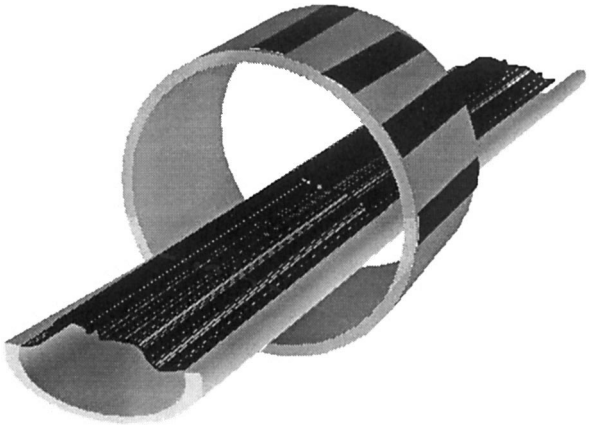

Fig. 1. Schematic diagram of laboratory capacitance electrode sensor installation around a section of a narrow rubber conveyor.

$$f(x) = a_0 + \sum_{i=1}^{N_S} a_{Si} \sin(ix) + \sum_{i=1}^{N_C} a_{Ci} \cos(ix) \quad (1)$$

where the number of sine terms N_S and of cosine terms N_C and the values of coefficients are selected by user. Note that a_0, odd a_{Si} and even a_{Ci} determine the symmetry of the solid distribution. Values other than zero a_0 and a_{Ci} return finite solid levels for $x = 0$ and $x = \pi$. Some examples of these profiles are given in Fig. 2. Of course, the Fourier series is not the only way of expressing $f(x)$ but it is convenient for our method of evaluation since in practice only the few first terms are taken into account, the series does not have to be orthogonal. In some cases, however, it is convenient to consider the full form.

A system of 12 electrodes was used, each 100 mm in length together with a set of driven guard electrodes to minimise terminal electric field fringe effects. Measurements from these electrodes yield 66 *sensitivity files* that contain the maps of *sensitivity distributions* based on a given reconstruction mesh and a 32×32 Cartesian mesh which was used to create the images. Two types of images will be referred to, as follows:

- 'real' images that correspond to the known and actual dielectric distribution (as the input for theoretical simulations described later); and
- 'reconstructed' images consisting of a mesh containing 1024 square pixels, 812 of them being placed in sensing area. Fig. 3 shows the arrangement, from which it can be seen that the electrode labelled as number 1 (of 12) placed between clock positions 2.30 and 3.30.

A number of experimental measurements indicated that the presence of the belt of reasonable thickness did not significantly affect the calibration procedure, which was based on collecting data with the belt empty and then 'full' of solids (see Section 3).

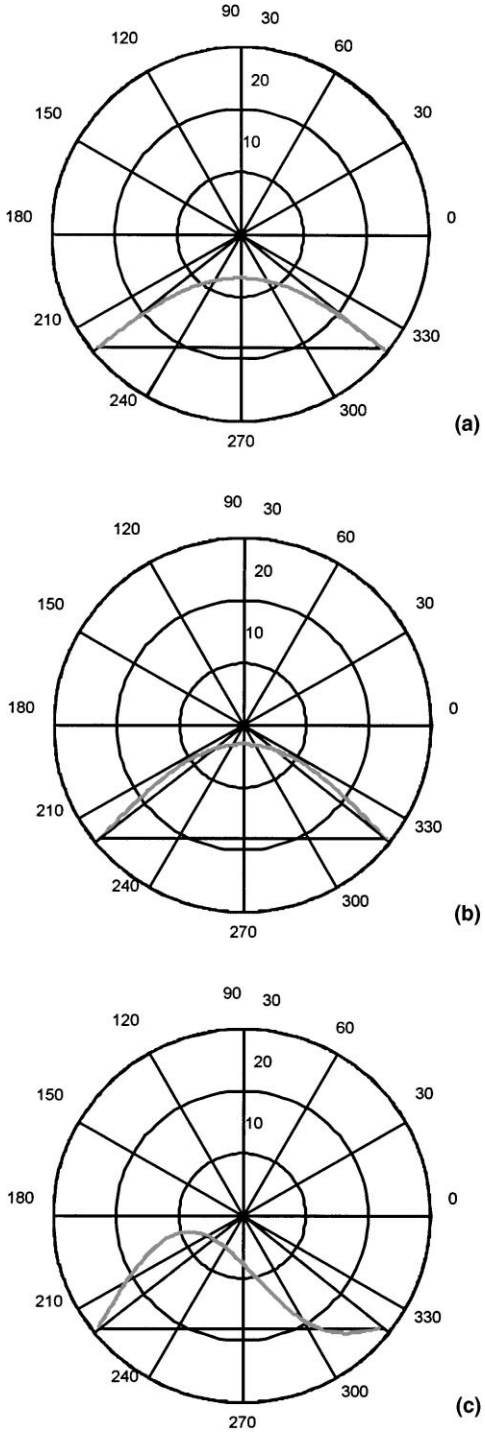

Fig. 2. Three examples of solid/gas interface profiles generated using Eq. (1) for which (a) (6 pixels)(sin(x)); (b) (8 pixels) (sin(x)), and (c) [(6 pixels)(sin(x) + (2 pixels)(sin(2x))].

2.3. Experimental variables

Since the geometry of the sensor cross-section arrangement may be normalised this was used to explore the effects of a number of parameters of interest (see Fig. 3). These were investigated by simulation and by direct experimental measurements:

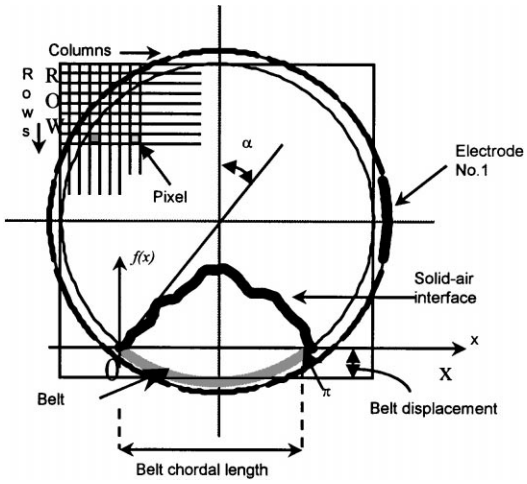

Fig. 3. Specification of belt and sensor arrangement used in experimental and simulation procedures.

- belt angle — α;
- ratio of belt thickness to its width (assuming initially that the cross-section of non-deflected belt is a rectangle);
- dielectric constant of the belt and the particulate solids.

Belt position is determined by angle α (Fig. 3), so its chordal length (in pixels) is given by:

$$\text{Chordal length} = 2\ \text{INT}\ (16 \sin(\alpha) + 0.5) \tag{2}$$

It corresponds with an x co-ordinate ranging from 0 to π. Various conditions were then investigated for these parameters as described below.

3. Theoretical simulations

To calculate the normalised dielectric constant first the maximum value is selected as the higher of solid and belt. Then, the normalised values are given by:

$$\varepsilon_{\text{N}} = \frac{\varepsilon - \varepsilon_{\text{minimum}}}{\varepsilon_{\text{maximum}} - \varepsilon_{\text{minimum}}} \tag{3}$$

where $\varepsilon_{\text{minimum}} = 1$ corresponds with the gas phase. Some examples of the real experimental images (though not necessarily presenting the most probable solids distribution that may be found in practical conveying) are given later.

The solution of the forward problem is completed in the second step of the simulation program and provides a set of 66 dimensionless capacitance, which are related to the data measured by the expression:

$$C_{\text{N}} = \frac{C - C_{\text{minimum}}}{C_{\text{maximum}} - C_{\text{minimum}}} \tag{4}$$

Note that in the *theoretical simulation* the calibration data remain unknown so C_{N} are calculated directly from the ε_{N} distribution corresponding with the real image and from the given set of sensitivity maps.

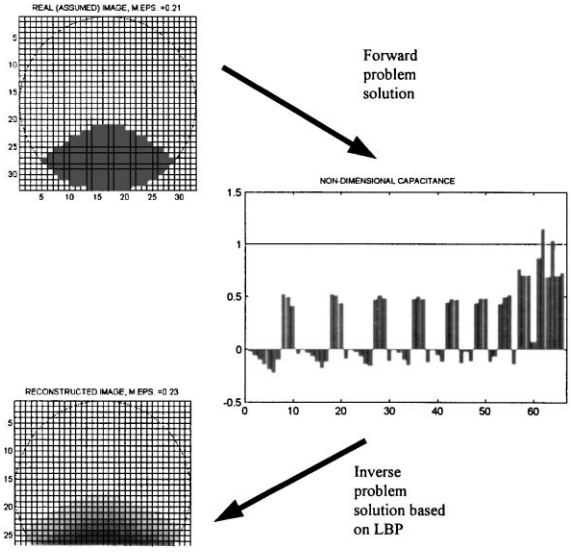

Fig. 4. Example of the steps in the dielectric field simulation for a belt conveyor for a solids profile corresponding to Fig. 2b.

Finally, the reconstructed image is obtained as a result of use of the equation:

$$\varepsilon_{\mathrm{NR}}(i,\,j) = \frac{\sum_{n=1}^{N-1}\sum_{m=n+1}^{N} C_{\mathrm{N}n,m} S_{n,m}(i,\,j) g_{n,m}}{\left\{\sum_{n=1}^{N-1}\sum_{m=n+1}^{N} S_{n,m}(i,\,j) g_{n,m}\right\}} \qquad (5)$$

where $\varepsilon_{\mathrm{NR}}(i,j)$ is the calculated normalised value of dielectric constant for pixel i, j, $S_{n,m}(i,j)$ is the corresponding value of sensitivity for n, m electrode connection (total number of them is equal to $N(N-1)/66$) and $g_{n,m}$ is a *weighting factor* of sensitivity map.

Fig. 4 shows an example of the simulation process corresponding to an input solids profile given by Fig. 2a, showing the forward solution to yield the non-dimensional capacitance values and the inverse problem solution, based on a linear back projection (LBP) algorithm.

4. Results

Some sample results will now be considered. In all cases, the experimental and simulation conditions considered a constant angle $\alpha = 51.3^{\circ}$ (which corresponds to a belt deflection equal to 6 pixel widths).

It became apparent that for the physically reasonable ratios of solids: belt dielectric constant the presence of belt itself does not affect the measured image for most scenarios considered. This is illustrated in Fig. 5, which shows response for two belt thicknesses and three dielectric constant ratios. The full set of data will be reported later. Other results will be reported later.

Fig. 6 shows the results for two different solid distributions (Fig. 2) as shown on the image in the left top corner in each of figure. The corresponding set of 66 dimensionless

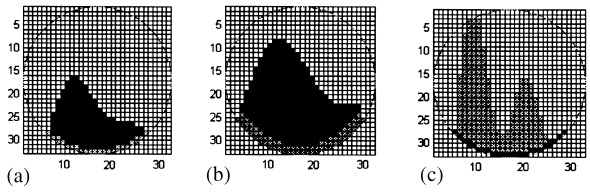

Fig. 5. Measured (real) images for profile given in Fig. 2c for different dielectric ratios and belt thickness: (a) thin belt (1 pixel thickness), $\varepsilon_{\mathrm{N}}(\mathrm{solid}) = 1$, $\varepsilon_{\mathrm{N}}(\mathrm{belt}) = 0.3$; (b) thicker belt (2 pixels thickness) $\varepsilon_{\mathrm{N}}(\mathrm{solid}) = 1$, $\varepsilon_{\mathrm{N}}(\mathrm{belt}) = 0.5$; (c) thin belt (1 pixel thickness) $\varepsilon_{\mathrm{N}}(\mathrm{solid}) = 0.4$, $\varepsilon_{\mathrm{N}}(\mathrm{belt}) = 1.0$.

capacitance is shown in the right, top corner of each figure. Below this (right) the *reconstructed* and *transferred* (bottom) images are depicted. Similarly on the left-hand side are shown the measured image and its transformation. It should be noted that the real images of theoretical and experimental simulations are not exactly the same. The discrepancies result not only from the accuracy of the experimental fabrication but also from the fact that the real image generated by the program is rounded (i.e. solid surfaces represent the step function).

The image transformation mentioned above is based on a simple operation. First the mean value of dielectric constant is calculated for measured and reconstructed images — $\langle\varepsilon\rangle$ and then the condition is followed:

$$\text{if } \varepsilon < \langle\varepsilon\rangle \text{ then } \varepsilon = 0 \text{ else } \varepsilon = 1 \qquad (6)$$

The theoretical simulation returns mean value closer to the assumed value than the experimental ECT measurement. The reason for this may be associated with under– and overshooting phenomena which can occur in ECT measurement and reconstruction, as discussed elsewhere [8]. The typical errors are only a few percent for the theoretical simulation, but increase up to several percent for measurement data. The procedure used now seems to be suitable and sufficiently robust to allow a measurement of the mean value of dielectric constant and, in most conditions, the form of the profile.

5. Conclusions and future research

The results of experimental and theoretical simulations indicate that ECT may have useful applications for on-line measurement on belt conveyors. It is evident that simulation procedures provide a proper estimate of the mean value of normalised dielectric constant and, thus the estimation of solid volume fraction in the sensing region. The calculated value can be corrected using a simple procedure based on a large number of straightforward measurements. Thus, the solid flow rate may be calculated, assuming that the belt velocity is known. The analysis of the shape of solids surfaces requires some further work to evolve a more comprehensive method of data processing. The preliminary results suggest

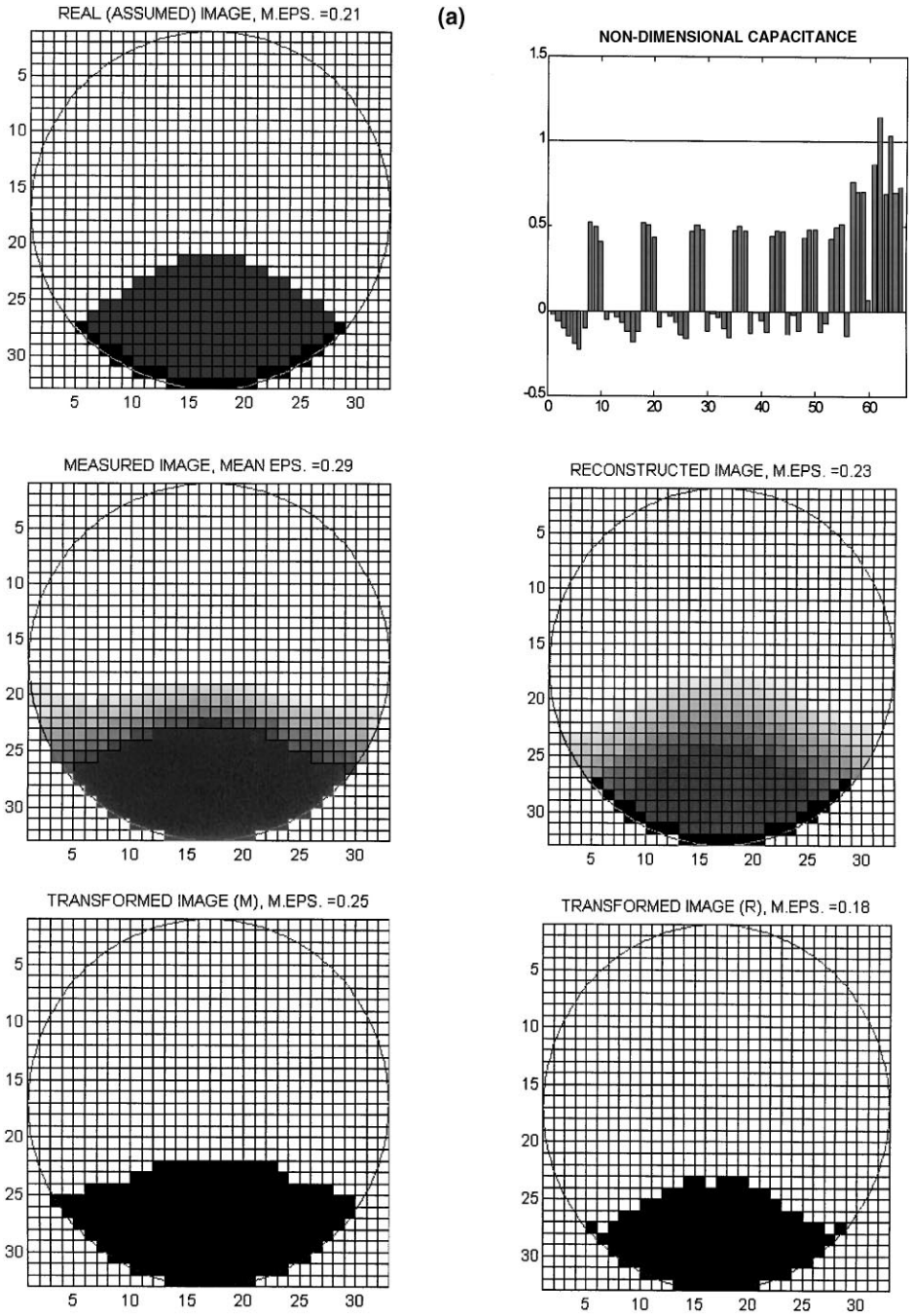

Fig. 6. (a) Examples of measured and simulated solids profiles on static belts (see text for description) corresponding to the case shown in Fig. 2a. (b) Examples of measured and simulated solids profiles on static belts (see text for description) corresponding to the case shown in Fig. 2c.

that the correction of the capacitance measurements could constitute a base for such analysis. A strategy based on direct (model-based) reconstruction to yield the equations of the parameters of the equation defining the profile seems to be the best route.

If the user has established confidence in the rendered image then, depending on the conveying application, two types of information will result from knowledge of the solids/gas profile. Firstly, if the profile is to be expressed in terms of the parameters defining a (smooth) fitting line then this gives the characteristic form of the solids at a given length scale. Second, if large particulates are being conveyed (e.g. >10% of belt diameter) then the form of the profile may not of course be smooth, in which case the discontinuities in the profile may be sensed by more detailed analysis of the image sets. For example, by collecting statistics of the contact perimeter estimated using different step lengths, or area sizes (which the pixelated image conveniently

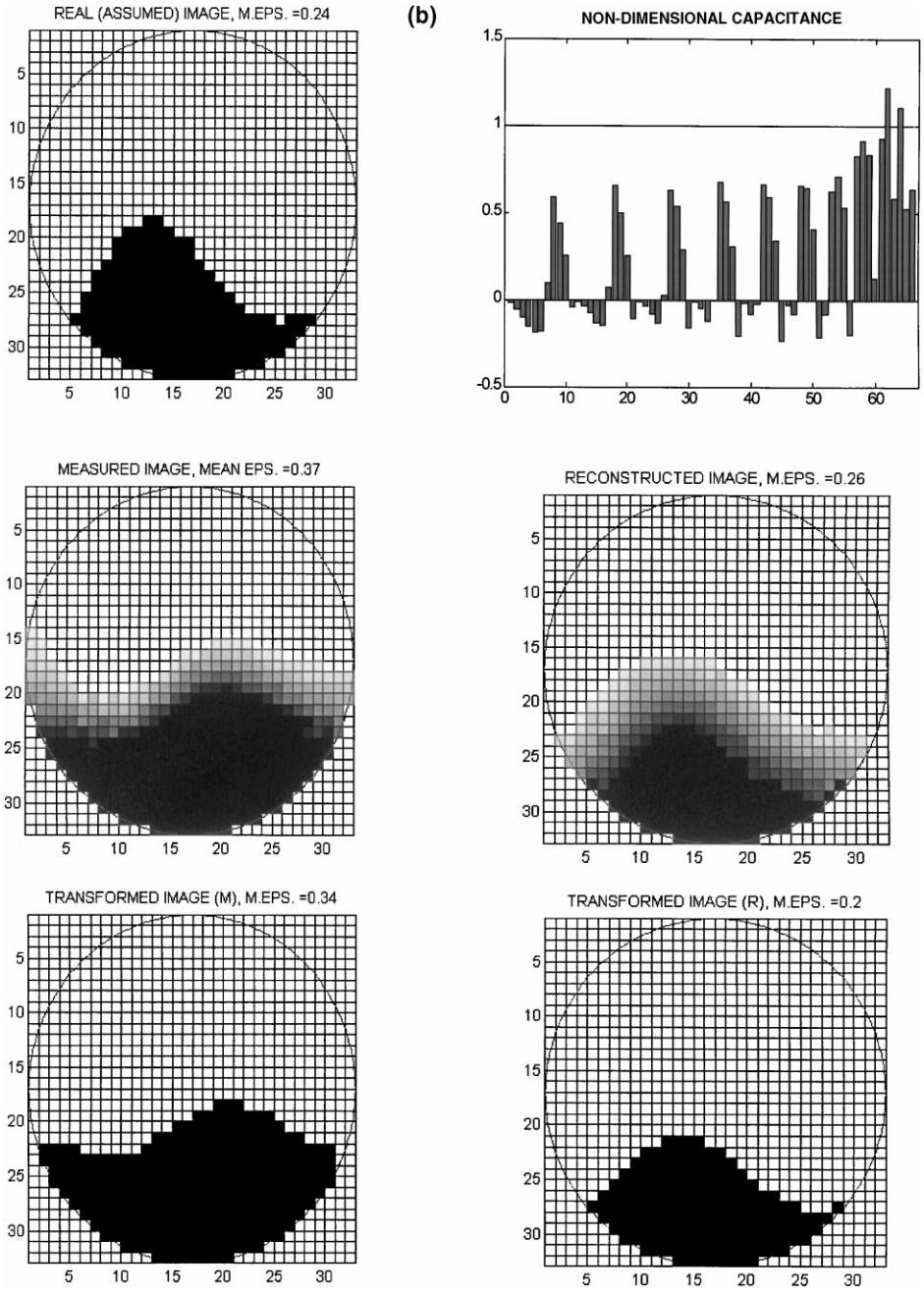

Fig. 6 (*Continued*).

provide) using methods that have been discussed elsewhere [9].

We suggest this information will be valuable to monitor feed streams (e.g. feed to crushers and grinding mills) and the quality of processed particulates (e.g. changes in shape of comminuted aggregates, changes in packing effects caused variations in fine particle shape, size or surface charge etc. as reflected in repose angle and its fluctuations with time). Some changes in humidity may also be detectable, but it should be kept in mind that dielectric constant is very sensitive to moisture content. For processes that experience variation in wetness factor some additional calibration procedure (procedures) may be required and this will in turn determine the size, position and measurement procedures used for the electrode sensitivity system. Alternatively, a set of calibration data may be input (for different wetness factors) and selection of the proper one may be achieved by means of a number of a simple logical operators. The question how to choose these operators for a given system remains to be addressed.

Future work will seeks to establish these applications and to examine in more detail other practical aspects associated with installation of ECT sensors in an industrial environment (air gaps, belt oscillation, etc).

References

[1] R.A. Williams, M.S. Beck (Ed.), Process Tomography, Principles, Techniques and Applications, Butterworth-Heinemann, Oxford, 1995.
[2] N. Reinecke, G. Petrisch, D. Schmitz, D. Mewes, Tomographic measurement techniques — visualization of multiphase flows, Chem. Eng. Technol. 21 (1998) 1–18.
[3] S.L. McKee, R.A. Williams, T. Dyakowski, T. Bell, T. Allen, Solid flow imaging and attrition studies in a pneumatic conveyor, Powder Technol. 82 (1995) 105–113.
[4] T. Dyakowski, R.B. Edwards, C.G. Xie, R.A. Williams, Application of capacitance tomography to gas–solid flows, Chem. Eng. Sci. 52 (1997) 2099–2110.
[5] S.J. Wang, T. Dyakowski, C.G. Xie, R.A. Williams, M.S. Beck, Real time capacitance imaging of bubble formation at the distributor of a fluidized bed, Chem. Eng. J. 56 (1995) 95–100.
[6] N. Reinecke, D. Mewes, Investigation of the two-phase flow in trickle-bed reactors using capacitance tomography, Chem. Eng. Sci. 52 (1997) 2111–2127.
[7] C.G. Xie, N. Reinecke, M.S. Beck, R.A. Williams, Electric tomography techniques for process engineering applications, in: M.S. Beck, et al. (Eds.), Process Tomography — A Strategy for Industrial Exploitation, UMIST/ECAPT/EU Brite Euram, Manchester, 1994, pp. 25–32.
[8] K.L. Ostrowski, S.P. Luke, R.A. Williams, Application of conjugate harmonics to electrical process tomography, Meas. Sci. Technol. 7 (1996) 316–324.
[9] B.H. Kaye, A Random Walk Through Fractal Dimensions, VCH (Weinheim), 1994, 427 pp.